the intermediate formation of species II, because coordination of CO to the vacant coordination site in II would compete with coordination of PR_3 at the site and the quantum yield would decrease. The quantum yield data in Table I show that the CCl_4 photoreaction becomes more efficient relative to the PR_3 photoreaction as the irradiation wavelength decreases. This result is entirely reasonable in the context of our proposal of two reaction channels, because relatively more radicals should be formed from the more energetic excited states.

The finding that the long-lived intermediate generated by flash photolysis reacts with CCl_4[7] coupled with our discovery that CCl_4 reacts with III to give only $CpFe(CO)_2Cl$ establish that it is not necessary to postulate 17-electron fragment intermediates as primary photoproducts based only on an observation that a chlorine abstraction product forms. In our scheme the chlorocarbon could react directly either with II or III (in the latter case by displacing phosphine) to give $CpFe(CO)_2Cl$, thereby explaining why $CpFe(CO)_2Cl$ is the only product in the photolysis of $Cp_2Fe_2(CO)_4$ with equimolar amounts of CCl_4 and PR_3. However, the fact that 6 atm of CO does not markedly inhibit the reaction with CCl_4 suggests that the reaction of II with chlorocarbons is not very efficient compared to the radical pathway.

The relatively long-lived photoproduct observed by Caspar and Meyer was proposed[7] to be $Cp_2Fe_2(CO)_3$, formed by Fe–CO bond dissociation. This particular photoproduct absorbs strongly in the visible, and it reacts with CO and other ligands. Because II should have a visible absorption band attributable to charge-transfer excitation from the coordinatively saturated iron to the 16-electron ("CpFeCO") center,[20] the flash photolysis results[7] can be accommodated equally well in terms of our mechanistic scheme.

Acknowledgment. We thank Dr. David Dooley and D. Jicha for assistance with certain experiments and Drs. T. J. Meyer and J. V. Caspar for sending us a preprint of their paper (ref 7). This research was supported by National Science Foundation Grants CHE78-10530 and CHE81-20419.

Registry No. $Cp_2Fe_2(CO)_4$, 12154-95-9; $Cp_2Fe_2(CO)_2(P(OMe)_3)_2$, 71579-40-3; $Cp_2Fe_2(CO)_3(P(O\text{-}i\text{-}Pr)_3)$, 33218-96-1; $CpFe(CO)_2Cl$, 12107-04-9; $Mn_2(CO)_{10}$, 10170-69-1; $(CO)_5Mn\text{-}Fe(CO)_2Cp$, 12088-73-2; Fe, 7439-89-6; $P(OMe)_3$, 121-45-9; PPh_3, 603-35-0; $P(n\text{-}Bu)_3$, 998-40-3; $P(O\text{-}i\text{-}Pr)_3$, 116-17-6; CCl_4, 56-23-5; $CHCl_3$, 67-66-3.

(20) As formulated, II would be expected to exhibit some degree of Fe(18-electron) → Fe(16-electron) charge transfer in its ground state. Thus, II could be viewed as a species in which there is metal–metal interaction of a donor–acceptor type. Relatively intense bands in the visible region are commonly observed in the absorption spectra of molecules that feature interactions of this sort.

Effects of Phenoxide Ligation on Iron–Sulfur Clusters. Preparation and Properties of $[Fe_4S_4(OAr)_4]^{2-}$ Ions and the Structure of $[(C_2H_5)_4N]_2[Fe_4S_4(OC_6H_5)_4]$

W. E. Cleland,[1a] D. A. Holtman,[1a,c] M. Sabat,[1b,d] James A. Ibers,[1b] G. C. DeFotis,[1e] and B. A. Averill*[1a,c]

Contribution from the Departments of Chemistry, Michigan State University, East Lansing, Michigan 48824, Northwestern University, Evanston, Illinois 60201, and the College of William and Mary, Williamsburg, Virginia 23185. *Received January 3, 1983*

Abstract: The phenoxide-ligated tetranuclear iron–sulfur clusters $[Fe_4S_4(OAr)_4]^{2-}$ (I, R = phenyl; II, R = *p*-tolyl) have been synthesized by reaction of $[Fe_4S_4(SR)_4]^{2-}$ or $[Fe_4S_4Cl_4]^{2-}$ with HOAr or NaOAr, respectively. The preparation, reactivity, and electronic properties of these compounds are described, as is the crystal structure of the Et_4N^+ salt of I. $[Et_4N]_2[Fe_4S_4(OPh)_4]$ crystallizes in the monoclinic space group C_{2h}^5—$P2_1/n$ with $Z = 4$ and unit-cell parameters $a = 17.610$ (4) Å, $b = 11.600$ (3) Å, $c = 22.810$ (6) Å, $\beta = 106.41$ (1)°, and $V = 4469.9$ Å^3 (−150 °C). The structure was refined to $R = 0.066$ and $R_w = 0.107$, using 6032 independent reflections with $F_o^2 > 3\sigma(F_o^2)$. The structure of I consists of an $[Fe_4S_4]^{2+}$ cubane core distorted toward D_{2d} symmetry, with a terminal phenoxide ligand completing the approximately tetrahedral coordination about each iron atom. The most notable structural feature is the short Fe–O distance (mean 1.865 (17) Å). Isotropically shifted resonances are observed in the ^1H NMR spectra of I and II; the directions and relative magnitudes of these shifts are consistent with significant delocalization of spin into the π system of the phenyl rings. At any temperature, the magnitude of the isotropic shifts is approximately twice that observed for the arenethiolate analogues. The magnitude of the isotropic shifts *increases* with increasing temperature, consistent with an antiferromagnetically coupled system. Variable-temperature magnetic susceptibility measurements are in agreement with the NMR data and give values of μ_{eff}/Fe of $\sim 1.3\mu_B$ at 25 °C. Zero field Mössbauer spectra of solid I show a single quadrupole doublet with parameters $\delta = 0.50$ and $\Delta E_Q = 1.21$ mm/s. Electrochemical data indicate that substitution of arenethiolate by phenolate ligands results in substantial *negative* shifts of first and second reduction potentials of the $[Fe_4S_4]^{2+}$ core. Reaction of I with PhSH, monitored by ^1H NMR spectroscopy, generates the mixed-ligand species $[Fe_4S_4(OPh)_{4-n}(SPh)_n]^{2-}$ (n = 0–4), with an approximately statistical distribution of ligands among the species present. The accumulated results are consistent with a relatively covalent Fe–O interaction in I and II. The biological implications for tyrosyl coordination to 4Fe–4S centers are discussed.

The iron–molybdenum protein of nitrogenase is now thought to contain two types of metal–sulfur clusters.[2-6] The iron–molybdenum cofactor[7-9] consists of a molybdenum–iron–sulfur cluster[10] whose structure is as yet unknown, depsite extensive

(1) (a) Michigan State University. (b) Northwestern University. (c) Current address: Department of Chemistry, University of Virginia, Charlottesville, VA 22901. (d) Current address: Department of Biochemistry, University of Wisconsin, Madison, WI 53706. (e) College of William and Mary.

(2) Zimmermann, R.; Münck, E.; Brill, W. J.; Shah, V. K.; Henzl, M. T.; Rawlings, J.; Orme-Johnson, W. H. *Biochim. Biophys. Acta* **1978**, *537*, 185–207.

(3) Huynh, B. H.; Henzl, M. T.; Christner, J. A.; Zimmerman, R.; Orme-Johnson, W. H.; Münck, E. *Biochim. Biophys. Acta* **1980**, *623*, 124–138.

0002-7863/83/1505-6021$01.50/0

studies employing a variety of spectroscopic techniques.[11-16] Because of the currently accepted hypothesis[5,6,17-20] that it is at the FeMo cofactor that substrates, including N_2, are reduced and because of the paucity of related inorganic structures, synthetic efforts to date have largely been directed at the preparation of Mo–Fe–S clusters as models for the FeMo cofactor.[6,20,21]

Cluster displacement studies using fluorinated thiols and ^{19}F NMR spectroscopic determination of Fe–S clusters,[22,23] cluster-transfer experiments using low molecular weight apoferredoxins to accept displaced Fe–S clusters followed by reduction and EPR spectroscopic quantitation,[24] and quantitation of the EPR spectra of the MoFe protein in partially denaturing organic solvents[25] have led to the conclusion that four tetrameric Fe–S clusters can be removed from the MoFe protein in addition to the FeMo cofactor.[4-6] These results are consistent with earlier EPR studies of CO-inhibited nitrogenase,[26] which detected EPR signals typical of 4Fe–4S centers in the net 1+ and 3+ oxidation states at low and high CO concentrations, respectively. ^{57}Fe Mössbauer spectra of MoFe protein from several species in the resting (as isolated) oxidation state show, in addition to the magnetic spectrum due to the cofactor centers, two quadrupole doublets in a 3:1 intensity ratio, accounting for 40 ± 2 and 13 ± 0.5% of the total iron present (twelve and four Fe atoms per molecule, respectively).[3,27,28] Because both species in strong applied magnetic fields behave as if they are diamagnetic, it has been proposed[2] that three iron atoms termed D (with a small quadrupole splitting) and one iron atom termed Fe^{2+} (with spectral parameters typical of high-spin iron(II) in a tetrahedral sulfur environment) together comprise a novel type of antiferromagnetically coupled tetranuclear Fe–S cluster, termed a P cluster. Studies of dye-oxidized MoFe protein[2,29] have shown that oxidation results in conversion of the D and Fe^{2+} components into a new magnetic species, P_{Ox}, with a ground state of high-spin multiplicity. MCD magnetization curves suggest an $S = {}^5/_2$ or ${}^7/_2$ ground state,[30] while preliminary magnetic susceptibility data support the $S = {}^5/_2$ value.[4] The apparent diamagnetism of the P clusters in the resting enzyme, the lack of MCD spectra characteristic of $[Fe_4S_4]^{2+}$ in the resting enzyme,[31] the high average isomer shift for species Fe^{2+} and D, and the oxidation of these entities by a single electron have led to the conclusion that the P clusters are a variant of normal 4Fe–4S clusters in the fully reduced, all-ferrous ($[Fe_4S_4]^0$) net oxidation state. The most likely means for the protein to differentiate the three iron atoms (D) from the fourth (Fe^{2+}) would be by use of non-thiolate ligands, such as tyrosyl phenolate or glutamate (or aspartate) carboxylate residues. At this point, however, it is impossible to rule out other possibile means of differentiation, such as addition of a fifth ligand or protein-imposed distortions of the clusters from their normal geometries.

Because of the limited data available on the P clusters, synthetic efforts aimed at developing possible model complexes have been few. Johnson and Holm[32] have generated in solution a carboxylate-substituted iron–sulfur tetramer and reported some of its spectroscopic properties, and we have briefly described[33] some properties of the phenoxide-ligated complex $[Et_4N]_2[Fe_4S_4(OPh)_4]$. In order to lay the groundwork for further studies of synthetic complexes that will be directly comparable to the protein-bound centers (the area of overlap between the protein centers and synthetically accessible Fe–S clusters appears to be at the $[Fe_4S_4]^+ = P_{Ox}$ level),[5,6] we describe herein the preparation and some properties of phenoxide-ligated $[Fe_4S_4]^{2+}$ clusters, including the structure of $[Et_4N]_2[Fe_4S_4(OPh)_4]$.

Experimental Section

Methods and Materials. All operations were carried out in an atmosphere of pure, dry dinitrogen that had been purified by passage over hot BASF catalyst R-3-11 and supported P_2O_5 (Aquasorb). Solvents and reagents were either distilled under an inert atmosphere or degassed by repeated evacuation and flushing with dinitrogen. Acetonitrile and propionitrile were distilled from CaH_2 and redistilled from P_2O_5. *N*-Methylpyrrolidinone was distilled from calcium hydride and then from barium oxide. Isopropyl alcohol was distilled from aluminum isopropoxide and tetrahydrofuran from lithium aluminum hydride. Phenols were either sublimed twice or sublimed followed by vacuum distillation. Sodium phenolates were prepared either by reaction with sodium methoxide in anhydrous methanol followed by evaporation of solvent in vacuo, addition of MeCN, and repeated evaporation to dryness or by reaction with metallic sodium in THF, followed by filtration and evaporation to dryness. Quaternary ammonium salts of $[Fe_4S_4(SR)_4]^{2-}$[34,35] (R = Et, *t*-Bu) and $[Fe_4S_4Cl_4]^{2-}$[36] were prepared by published procedures. Microanalyses were performed by Galbraith Laboratories, Inc., Knoxville, TN.

Physical Measurements. All samples were handled under anaerobic conditions. Optical spectra were obtained on either a Cary 219 or a Cary 17 spectrophotometer. ^1H NMR spectra were obtained on a Bruker

(4) Orme-Johnson, W. H.; Lindahl, P.; Meade, J.; Warren, W.; Nelson, M.; Groh, S.; Orme-Johnson, N. R.; Münck, E.; Huynh, B. H.; Emptage, M. Rawlings, J.; Smith, J.; Roberts, J.; Hoffmann, B.; Mims, W. B. In "Current Perspectives in Nitrogen Fixation"; Gibson, A. H., Newton, W. E., Eds.; Australian Academy of Science: Canberra, 1981; pp 79–83.

(5) Nelson, M. J.; Lindahl, P. A.; Orme-Johnson, W. H. In "Advances in Inorganic Biochemistry"; Eichhorn, G., Marzilli, L., Eds.; Elsevier: New York, 1982.

(6) Averill, B. A. *Struct. Bonding (Berlin)* **1982**, *53*, 59–103.

(7) Shah, V. K.; Brill, W. J. *Proc. Natl. Acad. Sci. U.S.A.* **1977**, *74*, 3249–3253.

(8) Burgess, B. K.; Jacobs, D. B.; Stiefel, E. I. *Biochim. Biophys. Acta* **1980**, *614*, 196–209.

(9) Burgress, B. K. in "Nitrogen Fixation: Chemical/Biochemical/Genetics Interface"; Müller, A., Newton, W. E., Eds.; Plenum Press: New York, 1982.

(10) Shah, V. K.; Brill, W. J. *Proc. Natl. Acad. Sci. U.S.A.* **1981**, *78*, 3438–3440.

(11) Rawlings, J.; Shah, V. K.; Chisnell, J. R.; Brill, W. J.; Zimmermann, R.; Münck, E.; Orme-Johnson, W. H. *J. Biol. Chem.* **1978**, *253*, 1001–1004.

(12) Huynh, B. H.; Münck, E.; Orme-Johnson, W. H. *Biochim. Biophys. Acta* **1979**, *527*, 192–203.

(13) Cramer, S. P.; Hodgson, K. O.; Gillum, W. O.; Mortenson, L. E. *J. Am. Chem. Soc.* **1978**, *100*, 3398–3407.

(14) Cramer, S. P.; Gillum, W. O.; Hodgson, K. O.; Mortenson, L. E.; Stiefel, E. I.; Chisnell, J. R.; Brill, W. J.; Shah, V. K. *J. Am. Chem. Soc.* **1978**, *100*, 3814–3819.

(15) Burgess, B. K.; Stiefel, E. I.; Newton, W. E. *J. Biol. Chem.* **1980**, *255*, 353–356.

(16) Burgess, B. K.; Yang, S.-S.; You, C.-B.; Li, J.-G.; Friesen, G. D.; Pan, W.-H.; Stiefel, E. I.; Newton, W. E. In "Current Perspectives in Nitrogen Fixation"; Gibson, A. H.; Newton, W. E., Eds.; Australian Academy of Science: Canberra, 1981; pp 71–74.

(17) Shah, V. K.; Chisnell, J. R.; Brill, W. J. *Biochem. Biophys. Res. Commun.* **1978**, *81*, 232–236.

(18) Newton, W. E. In "Kirk-Othmer: Encyclopedia of Chemical Technology", 3rd ed.; Wiley: New York, 1981, Vol. 15, pp 942–968.

(19) Mortenson, L. E.; Thorneley, R. N. F. *Annu. Rev. Biochem.* **1979**, *48*, 387–418.

(20) Holm, R. H. *Chem. Soc. Rev.* **1981**, *10*, 455–490.

(21) Coucouvanis, D. *Acc. Chem. Res.* **1981**, *14*, 201–209.

(22) Wong, G. B.; Kurtz, D. M., Jr.; Holm, R. H.; Mortenson, L. E.; Upchurch, R. G. *J. Am. Chem. Soc.* **1979**, *101*, 3078–3090.

(23) Kurtz, D. M., Jr.; McMillan, R. S.; Burgess, B. K.; Mortenson, L. E.; Holm, R. H. *Proc. Natl. Acad. Sci. U.S.A.* **1979**, *76*, 4986–4989.

(24) Rawlings, J. R.; Averill, B. A.; Orme-Johnson, W. H., unpublished observations.

(25) Orme-Johnson, W. H.; Davis, L. C.; Henzl, M. T.; Averill, B. A.; Orme-Johnson, N. R. Münck, E.; Zimmerman, R. In "Recent Developments in Nitrogen Fixation"; Newton, W., Postgate, J. R.; Rodriguez-Barrueco, C., Eds.; Academic Press: New York, 1977; pp 131–178.

(26) Davis, L. C.; Henzl, M. T.; Burris, R. H.; Orme-Johnson, W. H. *Biochemistry* **1979**, *18*, 4860–4869.

(27) Münck, E.; Rhodes, H.; Orme-Johnson, W. H.; Davis, L. C.; Brill, W. J.; Shah, V. K. *Biochim. Biophys. Acta* **1975**, *400*, 32–53.

(28) Smith, B. E.; Lang, G. *Biochem. J.* **1974**, *137*, 169–180.

(29) Smith, B. E.; O'Donnell, M. J.; Lang, G.; Spartalian, K. *Biochem. J.* **1980**, *191*, 449–455.

(30) Johnson, M. K.; Thomson, A. J.; Robinson, A. E.; Smith, B. E. *Biochim. Biophys. Acta* **1981**, *671*, 61–70.

(31) Stephens, P. J.; McKenna, C. E.; Smith, B. E.; Nguyen, H. T.; McKenna, M.-C.; Thomson, A. J.; Devlin, F.; Jones, J. B. *Proc. Natl. Acad. Sci. U.S.A.* **1979**, *76*, 2585–2589.

(32) Johnson, R. W.; Holm, R. H. *J. Am. Chem. Soc.* **1978**, *100*, 5338–5344.

(33) Cleland, W. E.; Averill, B. A. *Inorg. Chim. Acta* **1981**, *56*, L9–L10.

(34) Averill, B. A.; Herskovitz, T.; Holm, R. H.; Ibers, J. A. *J. Am. Chem. Soc.* **1973**, *95*, 3523–3534.

(35) Christou, G.; Garner, C. D. *J. Chem. Soc., Dalton Trans.* **1979**, *1093*–1094.

(36) Wong, G. B.; Bobrik, M. A.; Holm, R. H. *Inorg. Chem.* **1978**, *17*, 578–584.

WM-250 spectrometer. Magnetic susceptibility measurements were performed on an SHE Corp. SQUID susceptometer operating at 2 kG and on a modified PAR 155 vibrating sample magnetometer operating at 10 kG. Melting points were obtained in sealed tubes in vacuo and are uncorrected. Electrochemical measurements were performed on a PAR 174A polarographic analyzer, using either DC polarography (dropping mercury electrode) or cyclic voltammetry (platinum electrode); potentials are vs. the saturated calomel electrode. All solutions contained 50 mM $(Et_4N)(ClO_4)$ as supporting electrolyte. Mössbauer spectra were measured by Dr. T. Kent and Professor E. Münck at the Grey Freshwater Biology Institute, University of Minnesota; isomer shifts are reported vs. metallic Fe foil at room temperature.

Preparation of $[R_4N]_2[Fe_4S_4(OAr)_4]$ Salts. These complexes were prepared by either of two methods. Typical examples of each are described in detail below.

Method 1, from $[R_4N]_2[Fe_4S_4(SR')_4]$ (R' = Et, *t*-Bu). To 5.5 g (6.5 mmol) of $[Et_4N]_2[Fe_4S_4(SEt)_4]$ dissolved in 100 mL of MeCN was added a solution of 26 g (260 mmol) of PhOH in 75 mL of MeCN. The reaction mixture was evaporated in vacuo at 40 °C to ≤50-mL volume, diluted with 100 mL of MeCN, and again evaporated to a final volume of ≤50 mL. The color of the solution at this point was an orange-brown, rather than the green-brown of the starting material. Addition of 300 mL of *i*-PrOH to the filtered solution resulted in separation of the product as dark orange-brown microcrystals, which were collected by filtration, washed twice with *i*-PrOH, and vacuum dried. Recrystallization was accomplished by dissolution of the crude product in a minimum volume of MeCN at room temperature, filtration, addition of approximately 3 volumes of *i*-PrOH, and slow cooling to −20 °C, affording well-formed dark orange-brown prisms. The complex may also be recrystallized by dissolution in EtCN at 35 °C, filtration, and slow cooling to −20 °C. Typical yields are ~80% of analytically pure product after one recrystallization. Concentration of the mother liquors and slow cooling to −20 °C affords a second crop (~10%).

Method 2, from $[R_4N]_2[Fe_4S_4Cl_4]$. A mixture of 1.46 g (2.52 mmol) of $[Et_4N]_2[Fe_4S_4Cl_4]$ and 1.23 g (10.6 mmol) of anhydrous NaOPh was taken up in 80 mL of MeCN. An immediate color change from green-brown to orange-brown was observed, accompanied by formation of a white precipitate. The reaction mixture was stirred for 2 h and the precipitate removed by filtration and washed with a small portion of MeCN. The combined filtrate and wash were concentrated in vacuo until a dark crystalline precipitate began to form. Addition of several volumes of THF and cooling to −20 °C caused complete precipitation of the microcrystalline product, which was collected by filtration, washed with THF or *i*-PrOH, and recrystallized as in method 1 to give analytically pure product in ~85% yield. The product was found to be in all respects identical with that obtained by method 1.

$[Et_4N]_2[Fe_4S_4(OPh)_4]$ (I): mp 177 °C dec. Anal. Calcd for $C_{40}H_{60}Fe_4N_2O_4S_4$: C, 48.80; H, 6.14; Fe, 22.69; N, 2.84; O, 6.50; S, 13.03. Found: C, 48.49; H, 6.26; Fe, 22.08; O, 6.93; S, 13.14 (sample prepared by method 1).

$[Bu_4N]_2[Fe_4S_4(O\text{-}p\text{-}tol)_4]$ (II): mp 132 °C dec. Anal. Calcd for $C_{60}H_{90}Fe_4N_2O_4S_4$: C, 56.96; H, 7.97; Fe, 17.66; N, 2.21; S, 10.14. Found: C, 56.28; H, 7.79; Fe, 16.97; N, 1.92; S, 10.04 (sample prepared by method 1).

X-ray Analysis. Preliminary Weissenberg and precession photographs taken from a crystal sealed in a capillary under an argon atmosphere showed symmetry and systematic absences consistent with the monoclinic space group C_{2h}^5—$P2_1/n$. The crystal, of dimensions 0.23 × 0.29 × 0.51 mm, was mounted on a goniometer head in an argon-filled drybox and then transferred quickly under argon to the dry nitrogen cold stream of the diffractometer. Diffraction data at −150 °C were collected on a Picker FACS-1 diffractometer with graphite-monochromated Mo Kα radiation. Lattice parameters were obtained by automatic centering of 18 reflections within the range $0.3637 \leq \lambda^{-1} \sin\theta \leq 0.3851$ Å^{-1} with Mo Kα radiation (λ = 0.7093 Å). Intensities were corrected for absorption effects. Crystal data and details of data collection are given in Table I.

The procedures, atomic scattering factors, and anomalous dispersion corrections were used as previously described.[37] The early calculations were done on the Northwestern University CDC 6600 computer; later, the Lawrence Berkeley Laboratory CDC 7600 computer was used. The structure of the compound was solved by direct methods with the use of the MULTAN80 program. An *E* map showed positions of the atoms from the anion core (including several atoms from the phenyl rings) and also some atoms from cations. The remaining atoms were found from a weighted Fourier synthesis. The phenyl groups were constrained as rigid groups of D_{6h} symmetry with a C–C distance of 1.392 Å. The isotropic refinement of non-hydrogen atoms converged to values for *R* and R_w of 0.083 and 0.126, respectively. The positions of the hydrogen atoms of the rigid phenyl groups and of the methylene groups of the tetraethylammonium cations were calculated, while those of the methyl groups of the tetraethylammonium cations were located from difference electron density maps and idealized; the contributions of these atoms to the structure factors were fixed in subsequent refinements. Each hydrogen atom was given a *B* parameter 1.0 Å^2 greater than that of the carbon atom to which it is attached. The final, full-matrix, anisotropic, least-squares refinement of 319 variables with 6032 reflections with $F_o > 3\sigma(F_o)$ led to values of $R = 0.066$ and $R_w = 0.107$. The relatively high values of the *R* indices and the error in an observation of unit weight (3.14 e) may be a consequence of crystal quality, as inspection of the crystal after data collection revealed that some crystal faces were broken, possibly because of a phase change at low temperatures. However, the intensities of the standard reflections remained unaffected during data collection. The largest peak in the final difference electron density map is of height 1.2 (2) e/Å^3 and is near phenyl ring R(2). Five other peaks of height within the range 0.9 (2)–1.0 (2) e/Å^3 are in the iron–sulfur core. Final parameters for the nongroup atoms are listed in Table II and those for the rigid-group atoms in Table IS (supplementary material). Table IIS contains the values of $10|F_o|$ vs. $10|F_c|$.

Table I. Crystal Data and Data Collection Procedures for $[Et_4N]_2[Fe_4S_4(OC_6H_5)_4]$

formula	$C_{40}H_{60}Fe_4N_2O_4S_4$
fw, amu	984.6
space group	C_{2h}^5–$P2_1/n$
a, Å	17.610 (4)
b, Å	11.600 (3)
c, Å	22.810 (6)
β, deg	106.41 (1)
V, Å^3	4469.9
Z	4
temp, °C	~−150
cryst volume, mm^3	0.0244
radiation	graphite-monochromated Mo Kα, $\lambda(\alpha_1) = 0.7093$ Å
linear abs coeff, cm^{-1}	14.9
transmisn factors	0.688–0.761
detector aperture	5 mm wide, 6 mm high, 32 cm from crystal
takeoff angle, deg	2.6
scan speed	2.0° in 2θ/min
$\lambda^{-1} \sin\theta$ limits, Å^{-1}	0.0394–0.6180, $3.2° < 2\theta(\text{Mo K}\alpha_1) < 52.0°$
bkgd counts	10 s at each end of scan
scan range	0.8° below $K\alpha_1$ to 0.8° above $K\alpha_2$
data collected	$\pm h,k,l$
p	0.04
all data including systematic absences	8608
unique data with $F_o^2 > 3\sigma(F_o^2)$	6032

Results and Discussion

Synthesis of $[Fe_4S_4(OAr)_4]^{2-}$. The original synthesis reported for these complexes relied upon the observation[38] that solutions containing the thiolate-ligated clusters $[Fe_4S_4(SR)_4]^{2-}$ and excess phenol establish an equilibrium in which a small fraction of coordinated thiolate is displaced by phenolate (reaction 1). Use

$$[Fe_4S_4(SR)_4]^{2-} + \text{excess ArOH} \rightleftharpoons [Fe_4S_4(SR)_{4-n}(OAr)_n]^{2-} + \text{RSH} \quad (1)$$

of a cluster derived from a volatile thiol (e.g., EtSH, *t*-BuSH) allows the reaction to be driven to the right by repeated removal of solvent (and thiol) in vacuo. The resulting phenoxide-ligated clusters $[Fe_4S_4(OAr)_4]^{2-}$ are isolated in ~80% yield after purification by recrystallization. Although relatively convenient, method 1 has certain drawbacks, the most notable of which is the use of excess phenol to establish the initial equlibrium. In some cases we find that it is difficult to purify the phenolate tetramers because of their high solubility in organic solvents, especially the parent phenol, which makes precipitation with less polar solvents

(37) See, for example: Waters, J. M.; Ibers, J. A. *Inorg. Chem.* **1977**, *16*, 3273–3277.

(38) Que, L., Jr.; Bobrik, M. A.; Ibers, J. A.; Holm, R. H. *J. Am. Chem. Soc.* **1974**, *96*, 4168–4178.

Table II. Positional and Thermal Parameters for the Nongroup atoms of $[(C_2H_5)_4N]_2[Fe_4S_4(OC_6H_5)_4]$

ATOM	x	y	z	B_{11} or B, Å^2	B_{22}	B_{33}	B_{12}	B_{13}	B_{23}
FE(1)	0.001761(74)	0.19499(12)	0.135255(59)	10.13(44)	23.1(11)	6.85(29)	0.06(55)	3.05(28)	0.06(44)
FE(2)	-0.034501(77)	0.37508(12)	0.200757(61)	11.80(46)	18.9(10)	7.83(29)	-1.40(56)	3.01(29)	0.11(45)
FE(3)	-0.135701(73)	0.18935(12)	0.170777(60)	8.79(44)	21.5(11)	7.99(29)	-1.74(55)	2.41(29)	-0.29(45)
FE(4)	0.007132(75)	0.18421(12)	0.256475(60)	9.93(45)	22.6(11)	6.83(29)	0.31(55)	1.89(29)	0.70(44)
S(1)	-0.09524(14)	0.28569(21)	0.26271(11)	14.25(81)	25.5(19)	7.38(50)	2.74(98)	3.91(51)	-1.13(77)
S(2)	-0.04536(13)	0.04149(21)	0.17551(11)	11.37(77)	22.1(18)	7.90(48)	-0.23(94)	2.85(49)	-0.66(76)
S(3)	0.08603(13)	0.28067(21)	0.22045(11)	9.03(76)	29.6(20)	10.43(53)	-1.96(94)	2.90(52)	-0.15(80)
S(4)	-0.10650(14)	0.31581(22)	0.10477(11)	13.16(79)	28.3(19)	6.65(49)	1.3(10)	1.59(49)	0.19(79)
O(1)	0.04840(35)	0.16321(56)	0.07394(29)	11.1(22)	31.9(56)	12.2(15)	7.3(28)	8.9(15)	6.7(23)
O(2)	-0.02373(40)	0.53466(53)	0.20885(30)	22.4(27)	13.6(49)	10.7(16)	1.1(29)	5.1(17)	0.7(22)
O(3)	-0.23832(35)	0.13803(61)	0.16233(30)	7.5(21)	41.6(62)	11.5(16)	-5.0(29)	3.0(15)	-8.0(25)
O(4)	0.05107(36)	0.08126(57)	0.32943(28)	18.8(25)	27.3(55)	4.7(13)	3.2(29)	-1.2(15)	3.4(22)
N(1)	0.32200(44)	0.37076(71)	0.34507(35)	11.5(27)	29.5(67)	9.2(18)	-3.1(35)	3.3(18)	1.0(28)
N(2)	-0.16848(44)	-0.00518(69)	0.36091(37)	10.9(28)	17.7(63)	14.4(20)	4.1(34)	5.1(19)	2.6(29)
C(1)	0.34949(62)	0.3966(10)	0.28991(44)	22.7(40)	50.(10)	8.9(21)	-2.8(52)	5.2(24)	2.4(37)
C(2)	0.28930(70)	0.3861(12)	0.22914(55)	23.3(46)	76.(14)	16.0(29)	4.3(65)	12.4(31)	8.0(51)
C(3)	0.25143(56)	0.44910(93)	0.34494(51)	10.0(33)	40.9(88)	16.2(28)	-3.2(43)	5.1(25)	0.4(40)
C(4)	0.26759(58)	0.57631(95)	0.34111(55)	9.9(34)	39.4(90)	23.9(31)	2.5(44)	3.9(27)	1.1(42)
C(5)	0.29310(59)	0.24954(94)	0.34503(47)	19.9(37)	47.6(87)	8.0(24)	-14.0(46)	4.5(24)	0.9(37)
C(6)	0.35375(67)	0.15675(96)	0.34871(59)	24.7(44)	30.7(90)	23.9(34)	-5.6(49)	7.1(32)	-0.3(43)
C(7)	0.39033(54)	0.39370(93)	0.40091(45)	11.4(32)	39.8(91)	13.4(23)	-2.7(43)	3.6(22)	-2.9(37)
C(8)	0.37386(70)	0.3675(11)	0.46132(50)	25.5(47)	67.(12)	10.8(25)	2.1(60)	-2.6(27)	-5.0(44)
C(9)	-0.12207(61)	0.09283(94)	0.39787(45)	22.6(40)	40.4(91)	7.9(22)	-8.7(48)	0.5(24)	-2.7(36)
C(10)	-0.13980(75)	0.11586(99)	0.45803(53)	38.1(53)	34.0(93)	18.6(28)	-14.0(58)	12.8(32)	-2.2(41)
C(11)	-0.15637(60)	-0.11623(89)	0.39677(49)	22.4(38)	29.0(81)	13.1(26)	1.2(45)	9.5(26)	1.6(38)
C(12)	-0.07106(74)	-0.1497(11)	0.42344(57)	43.2(52)	68.(11)	17.0(32)	19.6(59)	11.6(33)	12.9(46)
C(13)	-0.14184(61)	-0.01639(89)	0.30378(46)	25.1(41)	32.3(84)	11.4(24)	-7.2(47)	12.1(27)	4.2(36)
C(14)	-0.18154(70)	-0.10837(98)	0.25902(50)	35.5(50)	41.9(92)	13.2(26)	-13.1(55)	11.3(30)	-3.3(40)
C(15)	-0.25515(56)	0.01909(95)	0.34449(50)	14.7(34)	43.1(94)	15.4(28)	-6.7(44)	5.8(25)	-4.0(40)
C(16)	-0.28239(67)	0.1287(11)	0.30979(53)	23.4(44)	67.(11)	15.5(28)	8.2(57)	4.1(29)	8.3(45)
H1C1	0.369	0.475	0.293	3.3					
H2C1	0.393	0.346	0.290	3.3					
H1C2	0.243	0.432	0.227	4.5					
H2C2	0.309	0.408	0.196	4.5					
H3C2	0.271	0.307	0.222	4.5					
H1C3	0.207	0.428	0.311	3.2					
H2C3	0.237	0.435	0.382	3.2					
H1C4	0.306	0.601	0.377	3.5					
H2C4	0.286	0.591	0.307	3.5					
H3C4	0.220	0.619	0.336	3.5					
H1C5	0.271	0.241	0.379	3.1					
H2C5	0.251	0.238	0.308	3.1					
H1C6	0.329	0.083	0.341	4.0					
H2C6	0.382	0.170	0.319	4.0					
H3C6	0.391	0.156	0.389	4.0					
H1C7	0.434	0.349	0.398	2.9					
H2C7	0.404	0.474	0.401	2.9					
H1C8	0.325	0.401	0.462	4.1					
H2C8	0.372	0.287	0.467	4.1					
H3C8	0.415	0.399	0.495	4.1					
H1C9	-0.067	0.077	0.406	3.2					
H2C9	-0.134	0.162	0.374	3.2					

ATOM	x	y	z	B, Å^2
H1C10	-0.123	0.192	0.472	4.0
H2C10	-0.194	0.108	0.454	4.0
H3C10	-0.111	0.082	0.488	4.0
H1C11	-0.180	-0.109	0.430	3.1
H2C11	-0.183	-0.177	0.370	3.1
H1C12	-0.067	-0.226	0.439	4.4
H2C12	-0.044	-0.146	0.392	4.4
H3C12	-0.046	-0.098	0.455	4.4
H1C13	-0.151	0.056	0.283	3.0
H2C13	-0.086	-0.031	0.316	3.0
H1C14	-0.238	-0.101	0.250	3.7
H2C14	-0.167	-0.102	0.222	3.7
H3C14	-0.166	-0.183	0.277	3.7
H1C15	-0.283	-0.044	0.321	3.3
H2C15	-0.271	0.023	0.382	3.3
H1C16	-0.261	0.195	0.334	4.1
H2C16	-0.265	0.131	0.274	4.1
H3C16	-0.339	0.134	0.298	4.1

[a] Estimated standard deviations in the least significant figure(s) are given in parentheses in this and all subsequent tables. [b] The form of the anisotropic thermal ellipsoid is $\exp[-(B(11)h^2 + B(22)k^2 + B(33)l^2 + 2B(12)hk + 2B(13)hl + 2B(23)kl)]$. The quantities given in the table are the thermal coefficients $\times 10^4$.

difficult. Most importantly, trace amounts of residual water or other impurities in the phenol apparently result in the formation of a new type of cluster compound characterized by a substantial shift of the lowest energy band in the optical spectrum to longer wavelength (by ~30 nm) and by significantly larger isotropic shifts in the ^{1}H NMR spectrum (vide infra). Further discussion of this material is deferred until an X-ray structural analysis is completed. It is possible, however, to minimize the likelihood of forming this alternative product simply by employing a ligand-exchange reaction (method 2) between the anhydrous sodium phenolate and an appropriate salt of $[Fe_4S_4Cl_4]^{2-}$ [36] (reaction 2).

$$[Fe_4S_4Cl_4]^{2-} + 4NaOAr \rightarrow [Fe_4S_4(OAr)_4]^{2-} + 4NaCl \quad (2)$$

Description of the Structure of $[Et_4N]_2[Fe_4S_4(OPh)_4]$. The structure of $[Et_4N]_2[Fe_4S_4(OPh)_4]$ consists of discrete cations and anions (eight and four per unit cell, respectively); the compound crystallizes in the monoclinic space group C_{2h}^5—$P2_1/n$ with one anion and two cations per asymmetric unit. Crystal data are given in Table I. The tetraethylammonium ions are not disordered, exhibit normal angles, distances, and ethyl group conformations, and will not be discussed further. The core structure is shown in Figure 1, along with the numbering scheme and selected interatomic distances. A stereoscopic view of the entire anion is shown in Figure 2, and a stereoscopic view of the unit cell along the b axis is given in Figure 1S. Positional and thermal parameters are listed in Table II and IS while values of $10|F_o|$ and $10|F_c|$ are compared in Table IIS (supplementary material). Selected interatomic distances and angles are listed in Table III, and best weighted least-squares planes are given in Table IV.

Figures 1 and 2 show clearly that the anion possesses the basic cubane structure found for other tetranuclear iron–sulfur dianions (e.g., $[Fe_4S_4(SCH_2Ph)_4]^{2-}$,[34] $[Fe_4S_4(SPh)_4]^{2-}$,[38] and $[Fe_4S_4Cl_4]^{2-}$).[39]

Table III. Bond Distances (A) and Angles (deg) for $[Et_4N]_2[Fe_4S_4(OC_6H_5)_4]$

Anion

Fe···Fe	
Fe(1)-Fe(2)	2.747 (2)
Fe(3)-Fe(4)	2.730 (2)
mean	2.739
Fe(1)-Fe(3)	2.762 (2)
Fe(1)-Fe(4)	2.763 (2)
Fe(2)-Fe(3)	2.756 (2)
Fe(2)-Fe(4)	2.759 (2)
mean	2.760 (3)
mean (of 6)	2.753 (13)

Fe-S	
Fe(1)-S(2)	2.266 (3)
Fe(2)-S(1)	2.252 (3)
Fe(3)-S(4)	2.263 (3)
Fe(4)-S(3)	2.253 (3)
mean	2.259 (7)
Fe(1)-S(3)	2.310 (3)
Fe(1)-S(4)	2.310 (3)
Fe(2)-S(3)	2.317 (3)
Fe(2)-S(4)	2.303 (3)
Fe(3)-S(1)	2.304 (3)
Fe(3)-S(2)	2.321 (3)
Fe(4)-S(1)	2.324 (3)
Fe(4)-S(2)	2.308 (3)
mean	2.312 (8)

Fe-S	
Fe(1)-S(1)	3.909 (3)
Fe(2)-S(2)	3.909 (3)
Fe(3)-S(3)	3.893 (3)
Fe(4)-S(4)	3.893 (3)
mean	3.901 (9)

S···S	
S(1)-S(2)	3.707 (3)
S(3)-S(4)	3.684 (3)
mean	3.696 (16)
S(1)-S(3)	3.586 (3)
S(1)-S(4)	3.569 (3)
S(2)-S(3)	3.573 (3)
S(2)-S(4)	3.593 (3)
mean	3.580 (11)

Fe-O	
Fe(1)-O(1)	1.848 (6)
Fe(2)-O(2)	1.865 (6)
Fe(3)-O(3)	1.860 (6)
Fe(4)-O(4)	1.888 (6)
mean	1.865 (17)

O-C(ring)	
O(1)-C(17)	1.359 (9)
O(2)-C(23)	1.342 (8)
O(3)-C(29)	1.355 (8)
O(4)-C(35)	1.353 (8)
mean	1.352 (7)

S-S-S	
S(4)-S(1)-S(3)	61.97 (7)
S(4)-S(2)-S(3)	61.87 (7)
S(1)-S(3)-S(2)	62.37 (7)
S(1)-S(4)-S(2)	62.34 (7)
mean	62.14 (25)
S(4)-S(1)-S(2)	59.15 (7)
S(3)-S(1)-S(2)	58.63 (6)
S(4)-S(2)-S(1)	58.51 (7)
S(3)-S(2)-S(1)	59.00 (7)
S(1)-S(3)-S(4)	58.78 (6)
S(2)-S(3)-S(4)	59.33 (6)
S(1)-S(4)-S(3)	59.25 (6)
S(2)-S(4)-S(3)	58.79 (6)
mean	58.97 (27)

O-Fe-S	
O(1)-Fe(1)-S(2)	116.2 (2)
O(1)-Fe(1)-S(3)	113.9 (2)
O(1)-Fe(1)-S(4)	113.5 (2)
O(2)-Fe(2)-S(1)	116.6 (2)
O(2)-Fe(2)-S(3)	112.8 (2)
O(2)-Fe(2)-S(4)	113.8 (2)
O(3)-Fe(3)-S(1)	106.9 (2)
O(3)-Fe(3)-S(2)	113.7 (2)
O(3)-Fe(3)-S(4)	122.4 (2)
O(4)-Fe(4)-S(1)	112.8 (2)
O(4)-Fe(4)-S(2)	111.3 (2)
O(4)-Fe(4)-S(3)	119.0 (2)
mean	114.4 (39)

Fe-S-Fe	
Fe(2)-S(1)-Fe(4)	74.13 (8)
Fe(2)-S(1)-Fe(3)	74.44 (9)
Fe(4)-S(1)-Fe(3)	72.30 (8)
Fe(1)-S(2)-Fe(3)	74.04 (9)
Fe(1)-S(2)-Fe(4)	74.32 (9)
Fe(3)-S(2)-Fe(4)	72.29 (8)
Fe(4)-S(3)-Fe(2)	74.25 (8)
Fe(4)-S(3)-Fe(1)	74.52 (9)
Fe(2)-S(3)-Fe(1)	72.82 (8)
Fe(3)-S(4)-Fe(1)	74.32 (9)
Fe(3)-S(4)-Fe(2)	74.25 (9)
Fe(1)-S(4)-Fe(2)	73.08 (8)
mean	73.7 (9)

Fe-Fe-Fe	
Fe(4)-Fe(1)-Fe(3)	59.23 (5)
Fe(4)-Fe(2)-Fe(3)	59.35 (5)
Fe(1)-Fe(3)-Fe(2)	59.70 (5)
Fe(1)-Fe(4)-Fe(2)	59.66 (5)
mean	59.49 (23)
Fe(4)-Fe(1)-Fe(2)	60.09 (5)
Fe(3)-Fe(1)-Fe(2)	60.05 (5)
Fe(4)-Fe(2)-Fe(1)	60.25 (6)
Fe(3)-Fe(2)-Fe(1)	60.26 (5)
Fe(2)-Fe(3)-Fe(4)	60.37 (5)
Fe(1)-Fe(3)-Fe(4)	60.40 (5)
Fe(2)-Fe(4)-Fe(3)	60.28 (5)
Fe(1)-Fe(4)-Fe(3)	60.37 (5)
mean	60.26 (13)
mean (of 12)	60.00 (41)

S-Fe-S	
S(2)-Fe(1)-S(3)	102.7 (1)
S(2)-Fe(1)-S(4)	103.5 (1)
S(3)-Fe(1)-S(4)	105.8 (1)
S(1)-Fe(2)-S(3)	103.4 (1)
S(1)-Fe(2)-S(4)	103.2 (1)
S(3)-Fe(2)-S(4)	105.7 (1)
S(1)-Fe(3)-S(4)	102.8 (1)
S(2)-Fe(3)-S(4)	103.2 (1)
S(1)-Fe(3)-S(2)	106.5 (1)
S(1)-Fe(4)-S(3)	103.2 (1)
S(2)-Fe(4)-S(3)	103.1 (1)
S(1)-Fe(4)-S(2)	106.3 (1)
mean	104.1 (15)

Fe-O-C(ring)	
Fe(1)-O(1)-C(17)	132.5 (5)
Fe(2)-O(2)-C(23)	128.7 (5)
Fe(3)-O(3)-C(29)	132.2 (6)
Fe(4)-O(4)-C(35)	122.6 (5)

Cations

N-C	
N(1)-C(1)	1.50 (1)
N(1)-C(3)	1.54 (1)
N(1)-C(5)	1.50 (1)
N(1)-C(7)	1.51 (1)
N(2)-C(9)	1.51 (1)
N(2)-C(11)	1.51 (1)
N(2)-C(13)	1.51 (1)
N(2)-C(15)	1.49 (1)
mean	1.51 (1)

C-C	
C(1)-C(2)	1.49 (2)
C(3)-C(4)	1.51 (2)
C(5)-C(6)	1.50 (2)
C(7)-C(8)	1.52 (2)
C(9)-C(10)	1.51 (1)
C(11)-C(12)	1.50 (2)
C(13)-C(14)	1.51 (2)
C(15)-C(16)	1.50 (2)
mean	1.51 (1)

C-N-C	
C(1)-N(1)-C(3)	109.4 (8)
C(1)-N(1)-C(5)	112.2 (8)
C(1)-N(1)-C(7)	107.7 (7)
C(3)-N(1)-C(5)	106.3 (7)
C(3)-N(1)-C(7)	110.4 (8)
C(5)-N(1)-C(7)	110.9 (8)
C(9)-N(2)-C(11)	111.6 (8)
C(9)-N(2)-C(13)	107.2 (7)
C(9)-N(2)-C(15)	110.6 (8)
C(11)-N(2)-C(13)	111.3 (8)
C(11)-N(2)-C(15)	106.0 (8)
C(13)-N(2)-C(15)	110.2 (8)
mean	109.5 (21)

N-C-C′	
N(1)-C(1)-C(2)	116.7 (8)
N(1)-C(3)-C(4)	114.3 (8)
N(1)-C(5)-C(6)	115.9 (8)
N(1)-C(7)-C(8)	114.8 (8)
N(2)-C(9)-C(10)	114.9 (8)
N(2)-C(11)-C(12)	114.3 (9)
N(2)-C(13)-C(14)	116.6 (8)
N(2)-C(15)-C(16)	116.3 (9)
mean	115.5 (10)

The specific distortions of the $[Fe_4S_4]^{2+}$ core are similar to those observed in related systems, namely, a compression of the core along an approximate 4 axis (through the top and bottom faces of the "cube" in Figure 1), resulting in a decrease in symmetry from idealized T_d toward D_{2d}. Key structural features include the following: (i) each face of the Fe_4S_4 core is a distinctly nonplanar rhomb (Table IV), with mean Fe–S–Fe and S–Fe–S angles of 73.7 and 104.1°; (ii) the Fe_4S_4 core can be viewed as being composed of interpenetrating Fe_4 and S_4 tetrahedra, the former being distinctly smaller and very close to a perfect tetrahedron, while the latter is significantly distorted from tetrahedral (the two S···S distances perpendicular to the $\bar{4}$ axis (mean 3.696 Å) are significantly longer than the four distances in the faces parallel to this axis (mean 3.580 Å); (iii) the distances and angles clearly divide into sets Fe–Fe and S···S (2 + 4), Fe–S (4 + 8), and Fe–Fe–Fe, S–S–S, S–Fe–S, and Fe–S–Fe (4 + 8) as expected for D_{2d} symmetry. These results and the comparative structural data given in Table V provide further evidence for the invariance of basic structural features of the $[Fe_4S_4]^{2+}$ core with a variety of terminal ligands to iron.

(39) Bobrik, M. A.; Hodgson, K. O.; Holm, R. H. *Inorg. Chem.* **1977**, *16*, 1851–1858.

Table IV. Least-Squares Planes for the Anion

(a) Coefficients $Ax + By + Cz - D = 0$

plane no.	A	B	C	D	plane no.	A	B	C	D
1	12.636	−1.215	10.443	1.201	7	10.229	7.418	−14.763	−0.478
2	6.760	−8.839	−13.886	−4.964	8	13.751	−7.101	−2.301	−3.684
3	2.398	−10.263	8.877	−0.774	9	4.264	5.336	17.132	5.374
4	16.929	0.301	−12.197	−2.939	10	13.801	−7.070	−2.424	−1.601
5	−4.315	−1.495	22.604	4.145	11	4.219	5.362	17.137	3.292
6	10.213	9.024	1.557	1.971	12	10.220	7.380	−14.865	−2.585

(b) Deviations ($\times 10^3$, in A) from Plane Number

	1	2	3	4	5	6	7	8	9	10	11	12
Fe(1)	−3 (1)		−22 (1)			17 (1)	−54 (1)			−81 (1)	79 (1)	
Fe(2)	4 (1)			19 (1)	−19 (1)		−56 (3)	84 (1)	−80 (1)			
Fe(3)		1 (1)	22 (1)		18 (1)			80 (1)			77 (1)	57 (1)
Fe(4)		−1 (1)		−19 (1)		−17 (1)			−73 (1)	−83 (1)		57 (1)
S(1)	−8 (2)		−54 (2)			44 (2)		−260 (2)	246 (2)			−185 (2)
S(2)	8 (2)			43 (2)	−44 (2)					256 (2)	−253 (2)	−181 (2)
S(3)		3 (3)	57 (3)		47 (2)		186 (2)		268 (2)	270 (2)		
S(4)		−3 (3)		−47 (2)		−46 (2)	185 (2)	−265 (2)			−253 (2)	

Table V. Comparison of Structural Parameters for Compounds with the $[Fe_4S_4]^{2+}$ Core

dist, A/angle, deg	$[Et_4N]_2[Fe_4S_4(SCH_2Ph)_4]$[a]	$[Me_4N]_2[Fe_4S_4(SPh)_4]$[b]	$[Et_4N]_2[Fe_4S_4Cl_4]$[c]	$[Et_4N]_2[Fe_4S_4(OPh)_4]$[d]
Fe-Fe	2.776 (2),[e] 2.732 (4)	2.730 (2), 2.739 (4)	2.755 (2), 2.766 (4)	2.739 (2), 2.760 (4)
Fe-S*	2.239 (4), 2.310 (8)	2.267 (4), 2.296 (8)	2.260 (4), 2.295 (8)	2.259 (4), 2.312 (8)
Fe-X	2.251	2.263	2.216	1.865
S*-S*	3.645 (2), 3.586 (4)	3.650 (2), 3.592 (4)	3.637 (2), 3.562 (4)	3.696 (2), 3.580 (4)
Fe-Fe-Fe	61.11 (4), 59.46 (8)	59.79 (4), 60.11 (8)	59.63 (4), 60.19 (8)	59.49 (4), 60.26 (8)
Fe-S*-Fe	73.8	73.5	74.6	73.7
S*-Fe-S*	104.1	104.3	103.5	104.1
S*-Fe-X	114.4	115.1	114.9	114.4
S*-S*-S*	61.11 (4), 59.45 (8)	61.08 (4), 59.47 (8)	61.41 (4), 59.30 (8)	62.14 (4), 58.97 (8)

[a] Reference 34. [b] Reference 38. [c] Reference 39. [d] This work. [e] Figures in parentheses are the numbers of values averaged where two distances or angles are given.

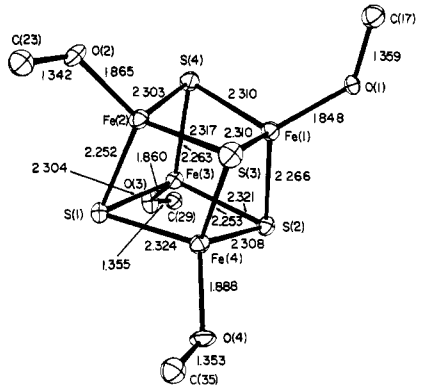

Figure 1. A portion of the $Fe_4S_4(OPh)_4$ core, showing 50% probability ellipsoids, the atom-labeling scheme, and interatomic distances.

Because relatively few tetrahedral iron complexes with phenoxide ligands have been structurally characterized, it is somewhat more difficult to assess the chemical implications of the iron phenoxide ligation in the $[Fe_4S_4(OPh)_4]^{2-}$ ion. The mean Fe–O bond distance of 1.865 (17) Å is intermediate between that found in the $[S_2MoS_2Fe(OPh)_2]^{2-}$ ion[40] (1.897 (27) Å; formally high-spin Fe(II)) and in the $[Fe(OAr)_4]^-$ ions[41] (1.847 (13) Å (Ar = 2,3,5,6-Me_4C_6H); 1.866 (6) Å (Ar = 2,4,6-$Cl_3C_6H_3$); both formally high-spin Fe(III)), as expected for an average Fe oxidation state of 2.5+ in I. The variation of Fe–O bond distances with iron oxidation state in these systems is relatively small and less than expected based on trends in ionic radius,[42] suggesting the presence of significant covalent character in the bond. Typical Fe(III)–O bond distances are longer than those observed here for monodentate phenoxide ligands (e.g., $[Fe(catecholate)_3]^{3-}$,[43] 2.02 Å; [Fe(salen)Cl][44] and $[Fe(salen)_2O]$[45] 1.88–1.92 Å). Some of this difference in metal–ligand distances arises from the expected effects of octahedral vs. tetrahedral coordination (e.g., the Fe(III)–Cl system[46]), but this does not satisfactorily account for the

Table VI. Electronic Spectral Features, Magnetic Moments, and Isotropic Shifts of Phenoxide Protons of $[Fe_4S_4(OAr)_4]^{2-}$ Complexes

	$[Fe_4S_4(OPh)_4]^{2-}$	$[Fe_4S_4(O\text{-}p\text{-}tol)_4]^{2-}$
electronic spectral features[a]	650 (sh), 410 (15.7), 270 (sh), 239 (44.0)	650 (sh), 424 (14.2), 270 (sh), 246 (42.2)
magnetic moment/iron (μ_{Fe}),[b] μ_B	1.32	1.25
isotropic shifts of phenoxide protons,[c] ppm	+2.31 (*o*-H), −2.23 (*m*-H), +2.86 (*p*-H)	+2.33 (*o*-H), −2.23 (*m*-H), −2.77 (*p*-CH_3)

[a] In acetonitrile solution at ~22 °C. λ_{max} (ϵ) in nm (M^{-1} $cm^{-1} \times 10^{-3}$). [b] In the solid state at ~23 °C. [c] In CD_3CN solutions at 22 °C, shifts vs. diamagnetic phenols. Chemical shifts downfield of Me_4Si are taken as negative.

(40) Teo, B.-K.; Antonio, M. R.; Tieckelmann, R. H.; Silvis, H. C.; Averill, B. A. *J. Am. Chem. Soc.* **1982**, *104*, 6126–6129.
(41) Koch, S. A.; Millar, M. *J. Am. Chem. Soc.* **1982**, *104*, 5255–5257.
(42) (a) Shannon, R. D.; Prewitt, C. T. *Acta Crystallogr., Sect. B* **1969**, *25B*, 925–946. (b) Shannon, R. D. *Acta Crystallogr., Sect A* **1976**, *32A*, 751–767.
(43) (a) Anderson, B. F.; Buckingham, D. A.; Robertson, G. B.; Webb, J. *Nature (London)* **1976**, *262*, 722–724. (b) Raymond, K. N.; Isied, S. S.; Brown, L. D.; Fronczek, F. R.; Nibert, J. H. *J. Am. Chem. Soc.* **1976**, *98*, 1767–1774.
(44) Gerloch, M.; Mabbs, F. E. *J. Chem. Soc. A* **1967**, 1598–1608.
(45) (a) Coggon, P.; McPhail, A. T.; Mabbs, F. E.; McLachlan, V. N. *J. Chem. Soc. A* **1971**, 1014–1019. (b) Gerloch, M.; McKenzie, E. D.; Towl, A. D. C. *Ibid.* **1969**, 2580–2588.

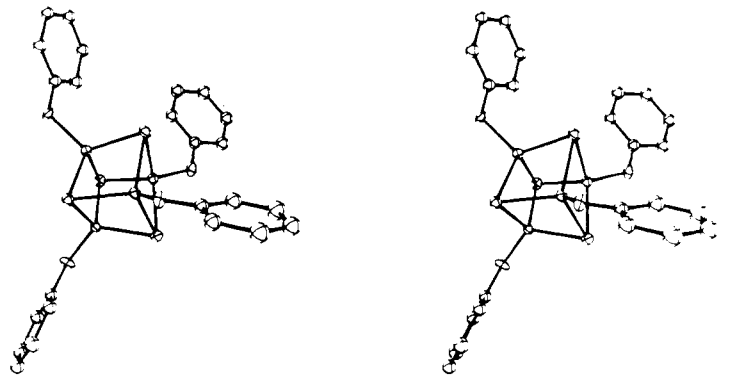

Figure 2. A stereoscopic view of the $[Fe_4S_4(OPh)_4]^{2-}$ ion. Probability ellipsoids are drawn at the 50% level. The hydrogen atoms are not included.

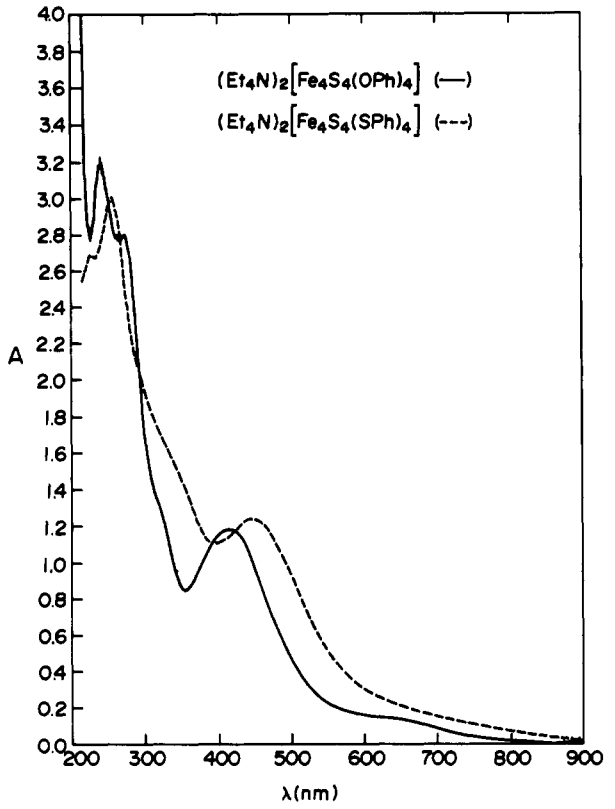

Figure 3. Electronic spectra of the $[Fe_4S_4(OPh)_4]^{2-}$ and $[Fe_4S_4(SPh)_4]^{2-}$ ions in acetonitrile solution at 22 °C.

unusally short Fe–O distances in I or $[S_2MoS_2Fe(OPh)_2]^{2-}$. Recent studies have shown, however, that coordination of phenolate to the *axial* position of a five-coordinate Fe(III) complex results in abnormally short Fe–O (phenolate) bonds[47] (e.g., Fe(saloph-(CatH)), 1.828 (4) Å; $[Fe(salen)]_2HQ$, 1.861 (2) Å ($CatH_2$ = catechol; HQ = *p*-hydroquinone dianion). One might view coordination of phenolate to the trigonal FeS_3 corner of a cubane as a situation somewhat analogous to the axial phenolate coordination in these five-coordinate Schiff base complexes. The Fe–O–C angles in I are slightly more acute than in the mononuclear $[Fe(OAr)_4]^-$ complexes[41] and in the Schiff base complexes.[47]

Electronic Spectra. The electronic absorption spectrum of I is compared with that of the thiolate analogue $[Fe_4S_4(SPh)_4]^{2-}$ in Figure 3; peak positions and extinction coefficients for typical $[Fe_4S_4(OAr)_4]^{2-}$ complexes are presented in Table VI. Several points are immediately apparent.

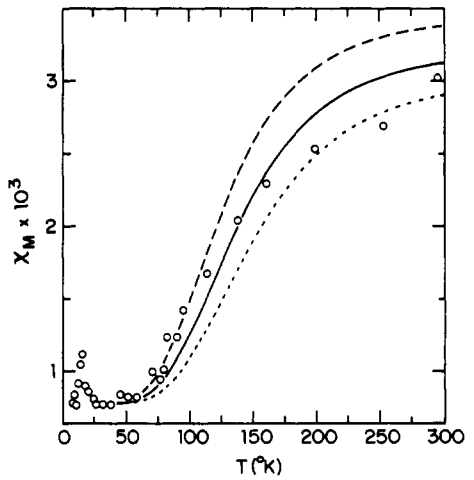

Figure 4. Magnetic susceptibility of solid $[Et_4N]_2[Fe_4S_4(OPh)_4]$ (O) as a function of temperature, compared to curves calculated (50a) for single J values of −160 (---), −175 (–), and −190 (···) cm^{-1}.

First, the spectra of the phenolate complexes are qualitatively very similar to those of the arenethiolate analogues,[48] with a significant blue shift of both the intense visible and ultraviolet bands (ca. 50 and 20 nm, respectively). This behavior is entirely consistent with the tentative assignment of the lower energy absorption as a terminal ligand-to-metal charge-transfer transition, inasmuch as substitution of a more electronegative oxygen atom for sulfur should increase the energy difference between metal and ligand orbitals. This behavior is in contrast to that observed for the carboxylate-ligated tetramer $[Fe_4S_4(OAc)_4]^{2-}$, which exhibits only a weak absorbance in the visible region rising steadily into the ultraviolet,[32] and is consistent with the greater degree of conjugation expected for a phenolate vs. a carboxylate oxygen.

Second, the spectra of the phenolate tetramers are much more sensitive to the effect of substituents on the aromatic ring than are those of the arenethiolate derivatives. Although the lability and difficulty in crystallization of the phenolate tetramers has thus far precluded the synthesis and spectroscopic examination of an extensive series of complexes with substituted phenolates, the effect of methyl substitution (a red shift of ~14 nm in the lowest energy band) is significantly larger than for the arenethiolate derivatives.[48,49] Finally, the feature at 600–700 nm is much better resolved in the spectra of the phenolate tetramers than in those of the arenethiolate analogues.[43] It corresponds in position and approximate intensity to similar features observed in the spectra of the halide-ligated tetramers,[36] suggesting that it arises from a transition within the $[Fe_4S_4]^{2+}$ core.

Magnetic Susceptibility. The magnetic susceptibility of I and II, measured on solid samples at room temperature, corresponds

(46) (a) Bennett, M. J.; Cotton, F. A.; Weaver, D. L. *Acta Crystallogr.* **1967**, *23*, 581–586. (b) Beattie, J. K.; Moore, C. J. *Inorg. Chem.* **1982**, *21*, 1292–1295.

(47) Heistand, R. H.; Roe, A. L.; Que, L., Jr. *Inorg. Chem.* **1982**, *21*, 676–681.

(48) DePamphilis, B. V.; Averill, B. A.; Herskovitz, T.; Que, L., Jr.; Holm, R. H. *J. Am. Chem. Soc.* **1974**, *96*, 4159–4167.

(49) Bobrik, M. A.; Que, L., Jr.; Holm, R. H. *J. Am. Chem. Soc.* **1974**, *96*, 285–287.

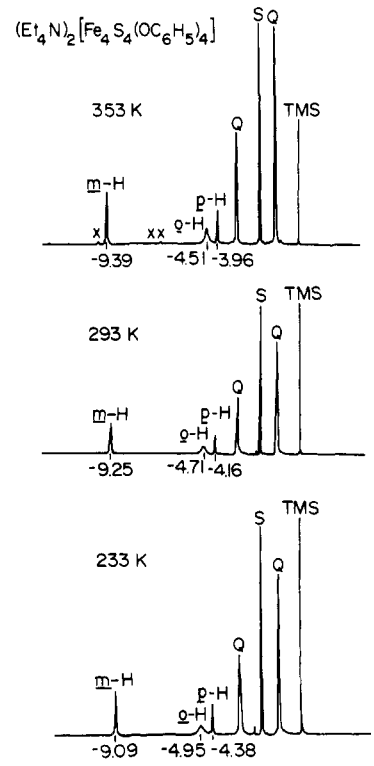

Figure 5. Proton magnetic resonance spectra (250 MHz) of $[Et_4N]_2[Fe_4S_4(OPh)_4]$ in CD_3CN solution at various temperatures. Peaks from protons of the cation are indicated by Q, solvent is indicated by S, and unidentified impurities are indicated by X. Chemical shifts are in parts per million from internal Me_4Si (TMS).

to effective magnetic moments of ca. 1.3 μ_B/iron atom, suggestive of intramolecular antiferromagnetic coupling. These values are virtually identical with those reported for thiolate[50,51] and halide[36] tetramers under similar conditions.

The susceptibility of I was measured from 4.2 to 300 K; the results, after the usual[36,50a,b] corrections for paramagnetic impurities at low temperatures and for diamagnetism, are plotted in Figure 4. The observed increase in susceptibility with increasing temperature above 50 K provides clear evidence for intramolecular antiferromagnetic spin coupling. The residual low-temperature peak in the curve is presumably due to inadequate impurity corrections using the normal Curie law approximation. The apparent value of 780 × 10^{-6} cgsu for TIP is higher than those found[36,50a,b] for the isoelectronic thiolate clusters (ca. 440 × 10^{-6} cgsu); it should be noted, however, that the apparent value of TIP is quite sensitive to the exact method used to correct for impurities. At any given temperature, the magnitude of μ/Fe for I is very similar to that observed for the halide and thiolate tetramer salts.[36,50a,b] Simulation of the data using a single J value[36,50a] provides the curves shown in Figure 4. It is apparent that no single J value adequately describes the experimental data; the discrepancies are similar to those observed for other tetramer salts using a similar analysis. The magnitude of $-J$ = 160–190 cm^{-1} is somewhat smaller than that estimated for the thiolate salts; in view of the uncertainty in the low-temperature data, however, a more detailed analysis (cf. ref 50b) was not attempted. The decreased value of J for I is, however, consistent with the increased ferrous character of the iron seen in the Mössbauer spectra (vide infra) and with the observation of substantially (~5×) smaller

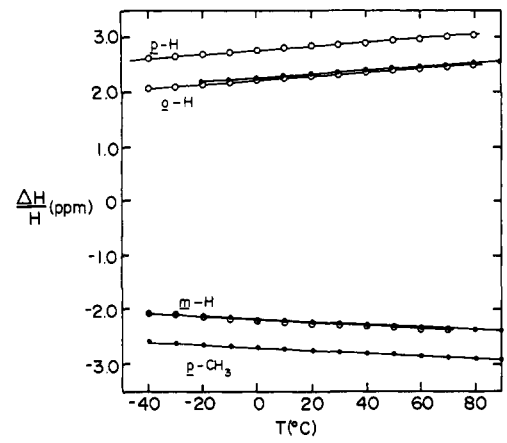

Figure 6. Temperature dependence of isotropically shifted ligand proton resonances of $[Et_4N]_2[Fe_4S_4(OPh)_4]$ (○) and $[Bu_4N]_2[Fe_4S_4(O\text{-}p\text{-}tol)_4]$ (●) in CD_3CN solution.

J values for compounds containing the $[Fe_4S_4]^+$ vs. the $[Fe_4S_4]^{2+}$ core (ref 50b).

Proton Magnetic Resonance. Proton magnetic resonance spectra have been measured for the phenoxide complexes I and II in acetonitrile as a function of temperature. In addition to the resonances of the cations, isotropically shifted resonances from the phenoxide protons are observed. Isotropic shifts at room temperature of the phenoxide protons are given in Table VI. Representative 250-MHz ^1H NMR spectra of I and II at various temperatures are shown in Figures 5 and 2S (supplementary material), while the temperature dependence of the isotropic shifts is shown in Figure 6.

In the phenoxide tetramer I, the meta protons are shifted to low field and ortho and para protons to high field (relative to the diamagnetic phenol). Assignments are based on the relative line widths and on the results of substitution of the p-H by CH_3. The ortho proton resonance at ca. 4.3–4.9 ppm is clearly identifiable by its relatively large line width, as dipolar broadening is expected to have an r^{-6} dependence.[52] Replacement of the p-H in I by CH_3 in II results in the disappearance of the peak at ca. −4 ppm and the appearance of a new peak at ca. −5 ppm with intensity corresponding to three protons. These results are qualitatively similar to those observed for the arenethiolate analogues[53] and suggest that dominant contact interactions are responsible for the observed isotropic shifts.

The only significant difference between the ^1H NMR spectra of the phenolate and arenethiolate tetramers is the magnitude of the observed shifts, which at any temperature are ca. twice as large for the phenolate derivative as for the corresponding arenethiolate complex. Since the magnetic properties of the two clusters are virtually identical, this difference must be due to a larger hyperfine interaction in the phenolate complexes. This is consistent with the structural data that suggest a relatively covalent Fe–O bond in these systems and inconsistent with a more ionic description of the bonding.

The observed isotropically shifted resonances are temperature dependent, with the magnitude of the shifts increasing with increasing temperature. The data are plotted in Figure 6, which demonstrates that, over the limited temperature range examined, the magnitude of the shifts parallels that of the magnetic susceptibility (Figure 4), again consistent with intramolecular antiferromagnetic coupling.

Mössbauer Spectra. The ^{57}Fe Mössbauer spectrum of I in the solid state at 4.2 K (Figure 3S; supplementary material) consists of a single quadrupole doublet with parameters δ = 0.50, ΔE_Q = 1.21, and Γ = 0.32 mm/s. Similar spectra are observed for

(50) (a) Laskowski, E. J.; Frankel, R. B.; Gillum, W. O.; Papaefthymiou, G. C.; Renaud, J.; Ibers, J. A.; Holm, R. H. *J. Am. Chem. Soc.* **1978**, *100*, 5322–5337. (b) Papaefthymiou, G. C.; Laskowski, E. J.; Frota-Pessoa, S.; Frankel, R. B.; Holm, R. H. *Inorg. Chem.* **1982**, *21*, 1723–1728. (c) Susceptibility of impurities was removed by a least-squares fit of the data between 20 and 60 K to $X = AT^{-1} + C$; the magnitude of the correction corresponds to ~0.4% high-spin Fe(III) impurity.

(51) Herskovitz, T.; Averill, B. A.; Holm, R. H.; Ibers, J. A.; Phillips, W. D.; Weiher, J. F. *Proc. Natl. Acad. Sci. U.S.A.* **1972**, *69*, 2437–2441.

(52) Horrocks, W. D., Jr. In "NMR of Paramagnetic Molecules: Principles and Applications"; LaMar, G. N., Horrocks, W. D., Jr.; Holm, R. H., Ed.; Academic Press: New York, 1973; Chapter 4.

(53) Holm, R. H.; Phillips, W. D.; Averill, B. A.; Mayerle, J. J.; Herskovitz, T. *J. Am. Chem. Soc.* **1974**, *96*, 2109–2117.

Table VII. Electrochemical Data for $[Fe_4S_4(OAr)_4]^{2-}$ Complexes

			DCP			DPP		CV		
compound	solv	process	$E_{1/2}$, V	slope, mV	i_d/C, μA/mM	E_p, V	$W_{1/2}$, mV	E, V	$E_{pc}-E_{pa}$, mV	i_{ap}/i_{cp}
$[Et_4N]_2[Fe_4S_4(OPh)_4]$	NMP	2−/3−	−1.15	−53	0.91	−1.17	111	−1.14	−132	1.07
	NMP	3−/4−	−1.80	−59	0.93	−1.83	125			
	MeCN	2−/3−	−1.08	−52	2.4			−1.08	−99	0.97
$[Bu_4N]_2[Fe_4S_4(O\text{-}p\text{-}tol)_4]$	NMP	2−/3−	−1.19	−49	0.69	−1.20	134	−1.18	−116	0.95
	NMP	3−/4−	−1.83	−53	0.92	−1.85	140			
	MeCN	2−/3−	−1.13	−47	1.67			−1.12	−93	0.99
	MeCN	3−/4−	−1.84	−52	1.83					
$[Et_4N]_2[Fe_4S_4(SPh)_4]$	NMP	2−/3−	−1.05	−52	1.05	−1.06	125	−0.99	−151	1.00
	NMP	3−/4−	−1.68	−52	0.95	−1.69	119			

both solid and frozen solution samples. The spectrum is not perturbed by an applied magnetic field of 600 G, as expected for an $S = 0$ system.

These results are completely comparable to those obtained for the arenethiolate tetramers,[54] except for the magnitude of the isomer shift, δ. For example, the corresponding parameters for salts of $[Fe_4S_4(SPh)_4]^{2-}$ at 4.2 K are $\delta = 0.46$ and $\Delta E_Q = 1.20$ mm/s.[54b] The increased isomer shift for I is consistent with increased "ferrous" character of the iron, again suggesting substantial covalent character to the Fe–O bond and increased donation of electron density from the phenoxide ligand (vs. thiolates) to the Fe_4S_4 core. Because phenoxide is inherently a poorer electron donor than thiophenoxide (cf. relative oxidizing power of PhOOPh vs. PhSSPh), this result is somewhat surprising, but it is consistent with the structural results presented above and the electrochemical data discussed below.

Electrochemical Studies. Differential pulse polarographic (DPP), dc polarographic (DCP), and cyclic voltammetric (CV) studies have been performed on ca. 1 mM solutions of I and II in acetonitrile and *N*-methylpyrrolidinone (NMP) over the potential range +1.0 to −2.0 V. No evidence for an oxidation process corresponding to formation of the $[Fe_4S_4(OAr)_4]^-$ monoanion, containing the $[Fe_4S_4]^{3+}$ core, was found in either case. Both complexes, however, undergo two relatively well-defined, quasi-reversible one-electron reduction reactions, corresponding to sequential formation of the tri- and tetraanions. Data for both compounds are presented in Table VII, and representative DPP and CV scans are illustrated in Figure 7.

As can be seen by comparison with the well-characterized $[Fe_4S_4(SPh)_4]^{2-}$ ion,[48] both the 2−/3− and 3−/4− processes approximate electrochemically reversible one-electron steps by any method used to examine them. Reduction potentials in NMP exhibit slight (≤0.07 V) negative shifts vs. acetonitrile, while DCP diffusion currents are reduced by a factor of approximately 2. The former effect occurs for thiolate clusters as well[48] (Table VII), and the latter may be due to the higher viscosity of NMP vs. MeCN. Substitution of the *p*-H by CH_3 results in a small (30–50 mV) negative shift in reduction potentials, as expected.[48]

Most importantly, the phenoxide-ligated tetramers exhibit the pattern of two one-electron reductions separated by ca. 600 mV that is typical of $[Fe_4S_4L_4]^{2-}$ complexes,[36,48] but the potentials for the two steps are negatively shifted by 100–150 mV vs. those of the arenethiolate analogues. Simple electronegativity arguments would predict that replacement of a sulfur donor by an analgous oxygen ligand should decrease the electron density on the $[Fe_4S_4]^{n+}$ core, rendering it more susceptible to reduction, as observed for $[Fe_4S_4(OAc)_4]^{2-}$ [32] and $[Fe_4S_4Cl_4]^{2-}$.[36] The fact that a shift in the opposite direction is observed suggests that, in this system at least, phenolate is capable of transferring more electron density to the $[Fe_4S_4]^{2+}$ core than thiophenolate, and is consistent with a relatively covalent Fe–O interaction. Similar results have been

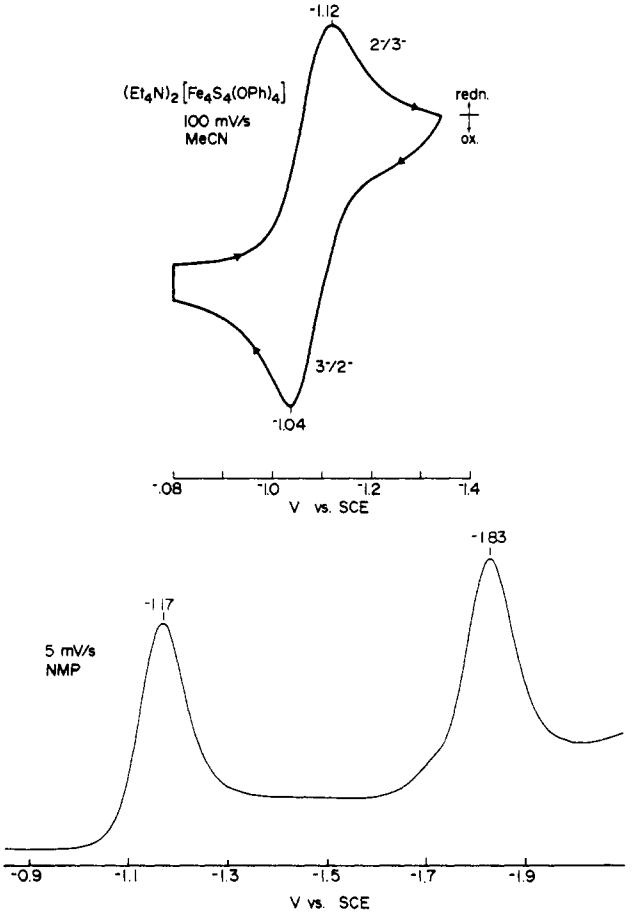

Figure 7. Cyclic voltammetry and differential pulsed polarography scans for $[Et_4N]_2[Fe_4S_4(OPh)_4]$. Solvents and scan rates are indicated.

observed for the $[S_2MoS_2FeL_2]^{2-}$ system (L = SPh,[52] OPh[55]).

Ligand-Exchange Reactions. The phenoxide cluster complexes are extraordinarily sensitive to trace amounts of water or other acidic impurities, making rigorous purification of solvents essential for the synthesis and for solution studies of spectroscopic properties. In addition, these materials are not stable for prolonged periods of time in solvents or solvent mixtures containing oxygen donors, such as *N*,*N*-dimethylformamide, *N*,*N*-dimethylacetamide, dimethyl sulfoxide, methanol, or THF (but not NMP). Whether this is due to solvoylsis by the pure solvents or to reaction with trace amounts of residual impurities is not clear, but this reactivity is comparable with that observed for the halide-ligated clusters $[Fe_4S_4X_4]^{2-}$ (X = Cl, Br, I).[36] Decomposition is accompanied by gradual loss of the longest wavelength absorption band and eventual formation of insoluble black precipitates.

The phenolate tetramers also react with electrophiles such as acyl halides, as shown by the quantitative formation of $[Fe_4S_4Cl_4]^{2-}$

(54) (a) Frankel, R. B.; Averill, B. A.; Holm, R. H. *J. Phys. (Orsay, Fr)* **1974**, *35*, C6-107–C6-112. (b) Because the isomer shifts reported in ref 54a are relative to that of Fe metal at the same temperature as the sample, we have remeasured the spectrum of $(Et_4N)_2[Fe_4S_4(SPh)_4]$ vs. Fe metal at room temperature and obtain the following parameters: $\delta = 0.46$ and $\Delta E_Q = 1.20$ mm/s.

(55) Silvis, H. C.; Averill, B. A. *Inorg. Chim. Acta* **1981**, *54*, L57–L58.

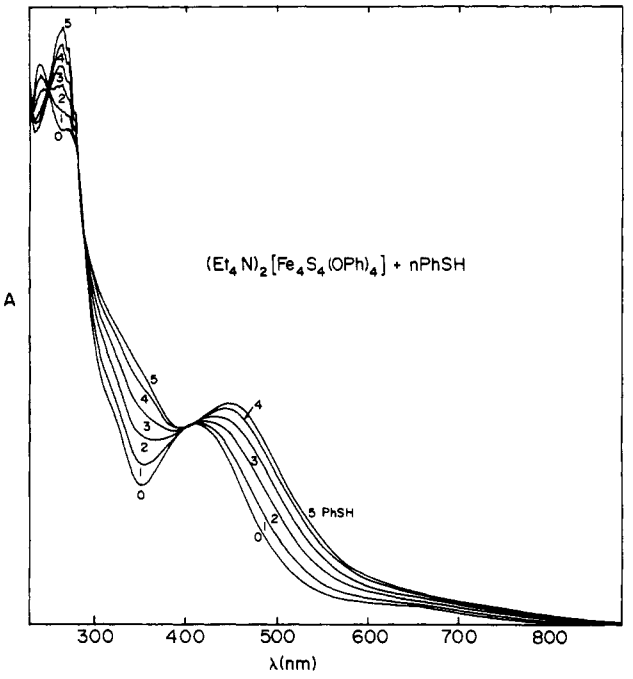

Figure 8. Optical spectra of a 3 mM solution of $[Et_4N]_2[Fe_4S_4(OPh)_4]$ in MeCN treated sequentially with 0–5 equiv PhSH at 22 °C (optical path length 0.2 mm).

Table VIII. Chemical Shifts[a] for Phenoxide and Thiophenoxide Ligands in $[Fe_4S_4(OPh)_{4-n}(SPh)_n]^{2-}$ Species (n = 0–4) in CD_3CN Solution at 22 °C

	n				
proton	0	1	2	3	4
m-H(PhO)	−9.25	−9.17	−9.10	−8.99	
p-H(PhO)	−4.15	−4.25	−4.34	−4.45	
m-H(PhS)		−8.38	−8.31	−8.25	−8.18
p-H(PhS)		−5.21	−5.24	−5.27	−5.29

[a] vs. Me_4Si (ppm).

(demonstrated by optical spectra) and phenyl benzoate upon treatment with benzoyl chloride (reaction 3). This reaction is completely analogous to that observed with the thiolate tetramer and acyl halides[32] but is somewhat surprising in light of the paucity of known examples of nucleophilic behavior of coordinated oxygen ligands.

$$[Fe_4S_4(OPh)_4]^{2-} + 4PhCOCl \rightarrow [Fe_4S_4Cl_4]^{2-} + 4PhCOOPh \quad (3)$$

Reaction of the phenolate tetramers with thiols such as thiophenol results in immediate and quantitative formation of the thiolate derivative (reaction 4), as expected from the evident lability of terminal phenolate ligands and the relative acidity of phenols and thiols.[38] These reactions have been demonstrated by monitoring optical and ^1H NMR spectra of the reaction mixtures.

$$[Fe_4S_4(OAr)_4]^{2-} + 4Ar'SH \rightarrow [Fe_4S_4(SAr')_4]^{2-} + 4ArOH \quad (4)$$

Optical spectra of a solution of $[Et_4N]_2[Fe_4S_4(OPh)_4]$ titrated with 0–5 equiv of PhSH are shown in Figure 8. The most notable effect of addition of PhSH is a progressive shift in the position of the lowest energy peak to longer wavelength, together with the appearance of a peak at ca. 260 nm with the concomitant disappearance of the original peak at 240 nm. Apparent isosbestic points are observed at 408, 398, 297, 290, and 248 nm. The final spectrum obtained upon addition of >4 equiv of PhSH is identical with that of the $[Fe_4S_4(SPh)_4]^{2-}$ ion[48] (cf. Figure 3).

Examination of solutions containing I and PhSH by ^1H NMR spectroscopy provides more detailed information on the nature of the species present; typical spectra are displayed in Figure 9.

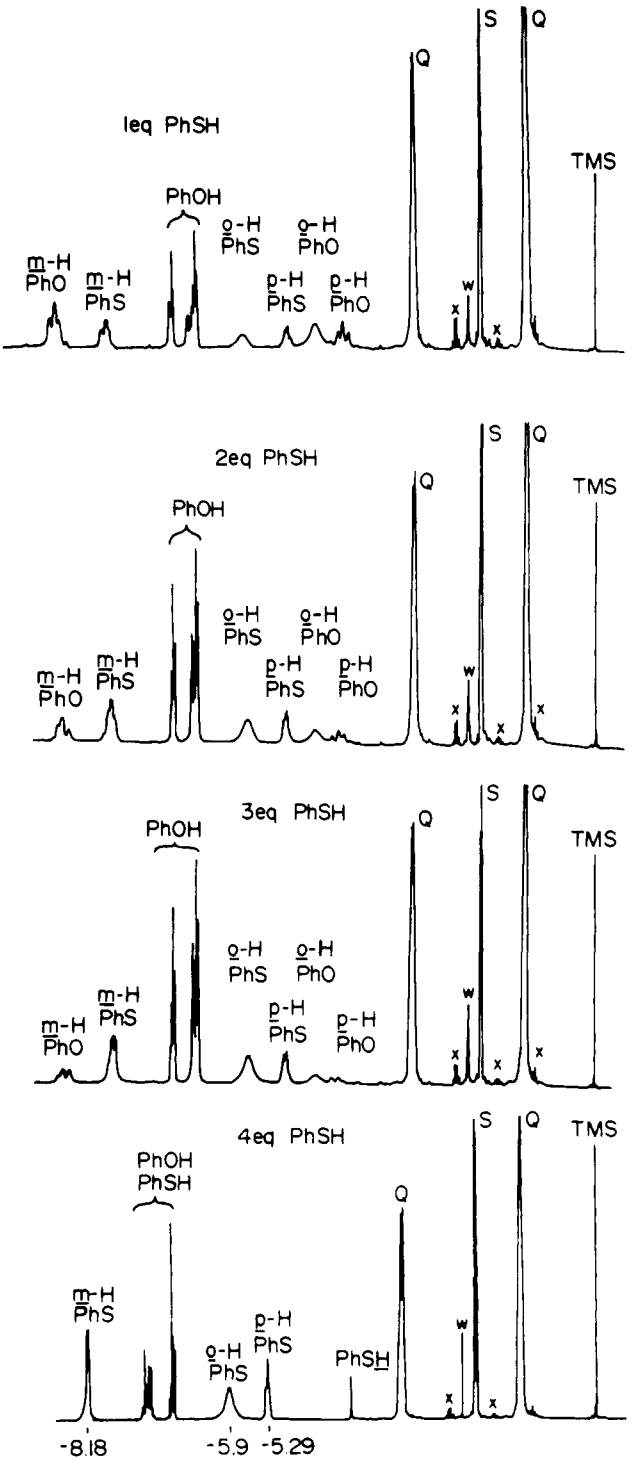

Figure 9. Proton magnetic resonance spectra (250 MHz) of a 10 mM solution of $[Et_4N]_2[Fe_4S_4(OPh)_4]$ treated sequentially with the indicated amounts of PhSH at 22 °C. Peaks from protons of the cation are indicated by Q, solvent is indicated by S, residual water is indicated by W, and unidentified impurities are indicated by X. Chemical shifts are in parts per million vs. Me_4Si internal standard (TMS).

Addition of n equiv PhSH ($n \leq 4$) results in the release of n equiv of free PhOH (estimated by integration vs. cation peaks), indicating that, as expected,[38] the more acidic thiol quantitatively displaces coordinated phenolate. In addition, the isotropically shifted proton resonances of coordinated phenolate decrease in the intensity and exhibit multiple peaks, while resonances typical of coordinated thiophenolate[53] appear at ca. −8.3 (*m*-H), −5.9 (*o*-H), and −5.2 (*p*-H) ppm. The variation in intensity of the peaks wtih PhS/PhO ratio allows the individual peaks to be assigned to the meta and para protons of the ligands in the mixed-ligand species $[Fe_4S_4(OPh)_{4-n}(SPh)_n]^{2-}$ (n = 0–4) (III); chemical shifts

Table IX. Ratios of Equilibrium Constants for PhS–PhO Exchange in CD_3CN Solution at 22 °C

$[PhSH]/[Fe_4S_4]$	K_4	K_5	K_6
	m-H(PhO)		
0.57	2.0	1.5	
0.89	2.5	2.6	
1.30	2.5	3.2	
1.67	2.6	2.8	
2.17	2.3	2.5	
2.77		2.7	
	m-H(PhS)		
1.30		2.5	3.7
1.67		2.5	2.8
2.17		2.7	2.5
2.77		3.4	2.7
average	2.4 (2)	2.7 (4)	2.9 (5)
statistical	2.66	2.25	2.66

are given in Table VIII. The line width of the ortho proton signals is greater than their chemical shift separation in the mixed-ligand species.

In view of the evidence for relatively covalent Fe–O interactions in I and the extreme difference in acidities of phenol and thiophenol, one might anticipate a nonstatistical distribution of ligands among the various species present. The relatively well-separated *m*-H and *p*-H signals of coordinated phenoxide provide a direct method of examining this. Concentrations of each of the species III (n = 0–4) were estimated by deconvolution of the partially resolved (*m*-H) peaks of coordinated phenolate and thiophenolate, determination of their relative areas, and comparison with the total integrated intensity (vs. cation protons as internal standard) of each set of peaks. Seven separate equilibrium constants are required to describe the situation, but only certain of these are independent.[38] The sequential substitution reactions are described by the equilibria K_n (n = 0–3).

$$K_n = \frac{[Fe_4S_4(OPh)_{4-(n+1)}(SPh)_{n+1}][PhOH]}{[Fe_4S_4(OPh)_{4-n}(SPh)_n][PhSH]}$$

Only the ratios $K_4 = K_0/K_1$, $K_5 = K_1/K_2$, and $K_6 = K_2/K_3$ can be determined independently.[38] Experimental values of K_4, K_5, and K_6 obtained at various PhSH:tetramer ratios are given in Table IX. The average values do not differ significantly from those calculated for a statistical distribution of ligands among the various species present. Similar statistical distributions of ligands have been observed for exchange of thiolate ligands with other thiolates,[38] and approximately statistical distributions are reported for mixed thiolate–acetate clusters as well.[32]

Conclusions. Coordination of phenoxide ligands to tetranuclear iron–sulfur clusters in place of arenethiolates gives the expected shift of optical spectral features to shorter wavelengths and has minimal effect on the magnetic properties of the $[Fe_4S_4]^{2+}$ core. Structural results showing somewhat shorter Fe–O bonds than expected, increased ^{57}Fe Mössbauer isomer shifts and isotropic shifts of ligand protons, and negative shifts of first and second reduction potentials all suggest that phenoxide ligands are capable of donating substantial electron density to the $[Fe_4S_4]^{2+}$ core, presumably via a relatively covalent Fe–O bond. This is not, however, reflected in any special stability of the phenoxide species, which are solvolyzed rapidly by substances with acidic protons.

These results, in particular the effect of phenoxide ligation on cluster oxidation–reduction properties, have certain biological implications. In nonaqueous solvents, phenoxide-ligated tetramers exhibit reduction potentials in the same range as tetramers with simple alkanethiolate ligands.[48] Previous work[56,57] has shown that incorporation of hydrogen-bonding functionalities such as peptide linkages into the ligands and use of mixed aqueous–organic solvents result in substantial positive shifts of the reduction potentials of thiolate tetramers, bringing them into the same range as is observed for small [4Fe–4S] ferredoxins under comparable conditions. Although the sensitivity of clusters such as I to solvolysis precludes examination in aqueous organic systems and substituted tyrosyl analogues of I are not yet available, the present results suggest that substitution of a cysteinyl thiol ligand to a [4Fe–4S] cluster in a protein by a tyrosyl phenoxide should have only a minor effect on cluster oxidation–reduction properties (in contrast to a carboxylate from an aspartate or glutamate residue, for which substantial (up to 400 mV[32]) positive shifts in reduction potentials are expected). Tyrosyl ligation would thus furnish a means of generating a reactive coordination site with minimal perturbation of cluster reduction potentials, possibly providing a site for interaction of a reducible substrate with the [4Fe–4S] core. Finally, the lability of coordinated phenoxide ligands and the similarity of optical spectra of phenoxide- and alkylthiolate-coordinated [4Fe–4S] clusters would seem to preclude detection of phenoxide [or carboxylate) ligation by cluster displacement (extrusion) methods[58,59] or by simple optical spectroscopy. To date, there is no direct evidence unequivocally demonstrating the presence of cluster ligands other than cysteine in any Fe–S protein.[60]

Acknowledgment. We thank Dr. T. Kent and Professor E. Münck for the Mössbauer spectra. This research was supported by grants from the Competitive Research Grants Office, Science and Education Administration, U.S. Department of Agriculture (B.A.A.; Grant No. 78-59-2261-0-1-175-1), and the National Institutes of Health (J.A.I.; Grant No. HL 13157). B.A.A. was an Alfred P. Sloan Foundation Fellow, 1981–1983.

Registry No. I, 79481-31-5; II, 86497-19-0; $[Fe_4S_4(OPh)_3(SPh)]^{2-}$, 86497-20-3; $[Fe_4S_4(OPh)_2(SPh)_2]^{2-}$, 86497-21-4; $[Fe_4S_4(OPh)(SPh)_3]^{2-}$, 86497-22-5; $[Et_4N]_2[Fe_4S_4(SPh)_4]$, 55663-41-7; $[Et_4N]_2[Fe_4S_4(SEt)_4]$, 76009-98-8; $[Et_4N]_2[Fe_4S_4Cl_4]$, 62758-02-5.

Supplementary Material Available: Derived parameters for the rigid-group atoms of $[Et_4N]_2[Fe_4S_4(OC_6H_5)_4]$ (Table IS), calculated and observed structure amplitudes (Table IIS), stereodiagram of the unit cell of $[Et_4N]_2[Fe_4S_4(OPh)_4]$ down the *b* axis (Figure 1S), proton magnetic resonance spectra of $[Bu_4N]_2[Fe_4S_4(O\text{-}p\text{-}Tol)_4]$ (Figure 2S), and Mössbauer spectrum of $[Et_4N]_2[Fe_4S_4(OPh)_4]$ (Figure 3S)(25 pages). Ordering information is given on any current masthead page.

(56) Que, L., Jr.; Anglin, J. R.; Bobrik, M. A.; Davison, A.; Holm, R. H. *J. Am. Chem. Soc.* **1974**, *96*, 6042–6048.
(57) Hill, C. L.; Renaud, J.; Holm, R. H.; Mortenson, L. E. *J. Am. Chem. Soc.* **1977**, *99*, 2549–2557.
(58) Averill, B. A.; Bale, J. R.; Orme-Johnson, W. H. *J. Am. Chem. Soc.* **1978**, *100*, 3034–3043.
(59) Wong, G. B.; Kurtz, D. M., Jr.; Holm, R. H.; Mortenson, L. E.; Upchurch, R. G. *J. Am. Chem. Soc.* **1979**, *101*, 3078–3090.
(60) Recent crystallographic results on a 7Fe-ferredoxin from *Azotobacter vinelandii*[61] and EXAFS studies on a 3Fe-ferredoxin from *Desulfovibrio gigas*[62] suggest that one of the ligands to the 3Fe–3S center in each may be an oxygen donor (tentatively identified as a water molecule in the former[61]).
(61) Ghosh, D.; Furey, W., Jr.; O'Donnell, S.; Stout, C. D. *J. Biol. Chem.* **1981**, *256*, 4185–4192.
(62) Antonio, M. R.; Averill, B. A.; Moura, I.; Moura, J. J. G.; Orme-Johsnon, W. H.; Teo, B.-K.; Xavier, A. V. *J. Biol. Chem.* **1982**, *257*, 6646–6649.